Optimal Auxiliary Frequency Control of Wind Turbine Generators and Coordination with Synchronous Generators

Ming Sun, *Student Member, IEEE*, Yong Min, Lei Chen, *Member, IEEE*, Kaiyuan Hou, Deming Xia, and Hangyin Mao

***Abstract*—Auxiliary frequency control of a wind turbine generator (WTG) has been widely used to enhance the frequency security of power systems with high penetration of renewable energy. Previous studies recommend two types of control schemes, including frequency droop control and emulated inertia control, which simulate the response characteristics of the synchronous generator (SG). This paper plans to further explore the optimal auxiliary frequency control of the wind turbine based on previous research. First, it is determined that the virtual inertia control has little effect on the maximum rate of change of frequency (Max-ROCOF) if the time delay of the control link of WTG is taken into consideration. Secondly, if a WTG operates in maximum power point tracking (MPPT) mode and uses the rotor deceleration for frequency modulation, its optimal auxiliary frequency control will contain only droop control. Furthermore, if the droop control is properly delayed, better system frequency response (SFR) will be obtained. The reason is that coordination between the WTG and SG is important for SFR when the frequency modulation capability of the WTG is limited. The frequency modulation capability of the WTG is required to be released more properly. Therefore, when designing optimal auxiliary frequency control for the WTG, a better control scheme is worth further study.**

***Index Terms*—Frequency droop control, power system frequency security, rate of change of frequency (ROCOF), virtual inertia control, wind turbine generator auxiliary frequency control.**

Nomenclature

Δf	System frequency deviation from rated frequency (50 Hz).
ΔP_{D}	Surplus power of the system.
T_{JS}	The inertia time constant of the synchronous generator (SG) rotor.
ΔP_{m}	SG power adjustment.
$K_{\mathrm{G,f}}$	Power–frequency static coefficient of SG.
T_{G}	The integrated time constant of prime mover and governor.
ΔP_{L}	Change in load power after disturbance.
$K_{\mathrm{L,f}}$	Power–frequency static coefficient of load.
K_{WD}	Coefficient of WTG frequency droop control.
K_{WI}	Coefficient of WTG virtual inertia control.
P_{Wm}	Wind power captured by the wind turbine.
$\Delta P_{\mathrm{We\_sig}}$	The control signal of WTG electric power change.
$P_{\mathrm{We0\_sig}}$	Reference of the control signal of WTG electric power.
$P_{\mathrm{We\_sig}}$	The control signal of WTG electric power.
P_{We}	The actual WTG output electric power.
P_{We0}	The initial WTG output electric power.
ΔP_{We}	The WTG output electric power adjustment.
T_{inv}	The inertia time constant of the converter.
ω_{W}	The rotor speed of WTG.
T_{JW}	The rotor inertia time constant of WTG.
ΔP_{D0}	System initial power disturbance.

Manuscript received March 19, 2020; revised May 28, 2020; accepted June 24, 2020. Date of online publication August 19, 2020; date of current version October 25, 2020. This work is supported by the National Natural Science Foundation of China (51922061) and the Science and Technology Project of State Grid Corporation of China (SGZJ0000KXJS1900418).

M. Sun, Y. Min and L. Chen (corresponding author, e-mail: chenlei08@tsinghua.edu.cn; ORCID: http://orcid.org/0000-0002-4778-4688) are with the State Key Laboratory of Control and Simulation of Power System and Generation Equipment, Department of Electrical Engineering, Tsinghua University, Beijing 100084, China.

K. Y. Hou and D. M. Xia are with Northeast Branch of State Grid Corporation of China, Shenyang 110180, Liaoning Province, China.

H. Y. Mao is with State Grid Zhejiang Electric Power Co. LTD., Hangzhou 310007, Zhejiang Province, China.

DOI: 10.17775/CSEEJPES.2020.00860

I. Introduction

As the penetration of renewable energy increases, traditional synchronous generators (SGs) are being replaced by renewable energy sources without the inertia or primary frequency control, such as wind turbine generators (WTGs) with doubly-fed induction generators (DFIG) or permanent magnet synchronous generators (PMSG), and photovoltaics (PV) [1]. The inertia and the frequency control capability of power systems have decreased significantly, and the frequency stability characteristics are worsening [2]. The above factors have become the main reason for restricting the further development of renewable energy.

To solve this problem, various control algorithms have been proposed. Auxiliary frequency regulation controllers have been added to WTGs. When system frequency rises, WTG output is reduced. When system frequency drops, if a WTG is operating in mode with reserve capacity, it increases its output [3], [4]. If a WTG is operating in maximum power point tracking (MPPT) mode, it increases its output only by decelerating its rotor speed and releasing the kinetic energy stored in the rotor [5]. When a WTG operates in MPPT mode, there are two main types of control strategies: frequency droop control (damping control) [6]–[10], and virtual inertia control (emulated inertia control) [10]–[15]. The frequency droop control emulates the primary frequency control of a SG. The input signal is the system frequency deviation, and the output signal is the wind turbine output power increment. The wind turbine output power increment changes linearly with the system frequency deviation [6]. Because this control scheme for wind turbines gives the wind turbine a control effect similar to that of SG damping, this control scheme is also called damping control. Virtual inertia control uses the frequency differential as an input signal [10], [11] and emulates the inertial response of a SG subjected to disturbances. In the initial stage of the system frequency response (SFR), the frequency deviation is small, while the frequency differential is relatively large. Thus, WTGs with virtual inertia control may provide quicker support power in the initial stage.

However, a WTG is quite different from a SG. Due to the delay effect in the internal control of a WTG, the control scheme, such as virtual inertia control, which was supposed to simulate the frequency response of a SG, may not be able to achieve the desired effect. At the same time, for the sake of the cost, a WTG usually operates in MPPT mode and uses the acceleration or deceleration of the rotor to participate in the frequency modulation of the system. When the system frequency drops, due to the minimum speed limit of the WTG, the frequency modulation ability of the WTG is limited. System frequency will drop again when the WTG rotor speed limit is reached and the WTG terminates the auxiliary frequency control mode [3], [16]. Moreover, the primary frequency control (PFC) of a SG reacts to the frequency deviation relatively slowly. Therefore, the quick release of the limited energy stored in the rotor with the virtual inertia control is not helpful for the action of PFC of a SG in the initial stage and is not always the best strategy. Coordination between the WTG and SG must be taken into consideration when designing optimal auxiliary frequency control for the WTG [17].

Based on the existing research, this paper explores a better design idea for the auxiliary frequency control scheme of a WTG and makes a preliminary exploration of some specific scenarios. The main contributions of this paper are as follows:

1) When the delay effect in the internal control of a WTG is considered and approximated as the first order inertial link, the virtual inertia control of the WTG has little effect on the maximum rate of change of frequency (Max-ROCOF).

2) If a WTG operates in maximum power point tracking (MPPT) mode and uses the rotor deceleration for frequency modulation, its optimal auxiliary frequency control will contain only droop control. The reason is that the quick release of limited energy stored in the WTG rotor in the initial stage of SFR will restrain the release of the PFC for the SG. The coordination of the WTG and SG is necessary.

3) Furthermore, if a first-order inertial segment is added in the frequency droop control of the WTG, SFR can be even better, which further validates that the frequency modulation capability of the WTG is required to be released at a proper speed. Therefore, a more proper control scheme of the WTG is worth further investigation.

The remainder of the paper is organized as follows. Section II introduces our detailed analysis model. Section III discusses the effect of virtual inertia control on Max-ROCOF. Section IV studies the optimal auxiliary frequency control of a WTG. Section V further enhances the auxiliary frequency control of a WTG and discusses the importance of coordination between the WTG and SG. Section VI presents the conclusions.

II. Model Description

To simplify the analysis, we assume that the whole system has the same frequency. The frequency dynamics in any node or generator are all the same. Therefore, the simplified system model including only one SG, one WTG, and one load is used to analyze system frequency response [13], [18]–[21]. The model is a revision of the classic SFR model using a WTG with auxiliary frequency control added [18].

The block diagram of the system is shown in Fig. 1.

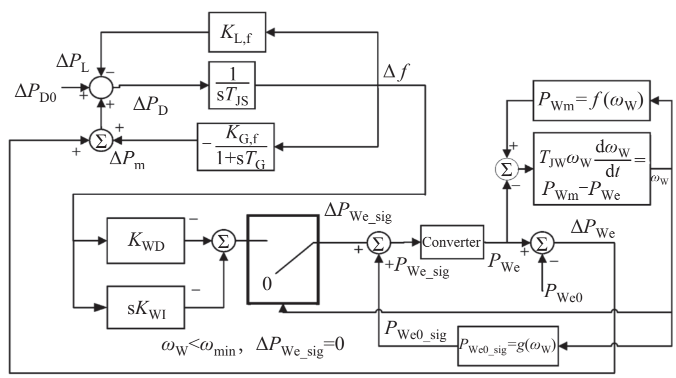

Fig. 1. Block diagram of the system.

The model of the WTG includes rotor dynamics, an aerodynamic model of the wind turbine, MPPT control, and auxiliary frequency control.

Here, we only discuss the severe situation in which the power system encounters a power shortage, and the system frequency drops. For economic reasons, we assume that the WTG operates in MPPT mode, and that it can only provide temporary support for the system frequency [16].

Under these circumstances, when the WTG engages in frequency regulation, it increases its output electric power, and therefore its rotor slows down because the output electrical power is greater than the input mechanical power. When the speed of the wind turbine is less than a certain value, the wind power captured by the wind turbine drops sharply, which may cause the wind turbine to stop. For the WTG to avoid a shutdown, its rotor has a minimum speed limit. When its rotor speed reaches the minimum speed limit, the WTG terminates the auxiliary frequency control mode and its rotor accelerates to the maximum power point again. The process of a WTG terminating the system frequency regulation may cause the system frequency to drop again [16]. This process must be considered.

To describe the entire process of a WTG participation in power system frequency regulation more clearly, Fig. 2 is presented. In the initial stage, the WTG operates at point A. The mechanical power it obtains from the wind is equal to the electric power it outputs to the grid. Then, a power disturbance occurs in the grid. Considering the worst situation, we assume the power disturbance to be a sudden power shortage. Thus, the electric power that the WTG outputs to the grid increases. The WTG engages in the primary frequency regulation process and increases its electric power output. It now changes to operate at point B, where its electric power output is bigger than the mechanical power input, and the rotor begins to decelerate. When the rotor speed decelerates to a minimum speed limit (point C), the WTG terminates the auxiliary frequency control mode. Thus, WTG comes to point D. The mechanical power input is now bigger than the electric power output, and the rotor begins to accelerate. Finally, WTG returns to point A.

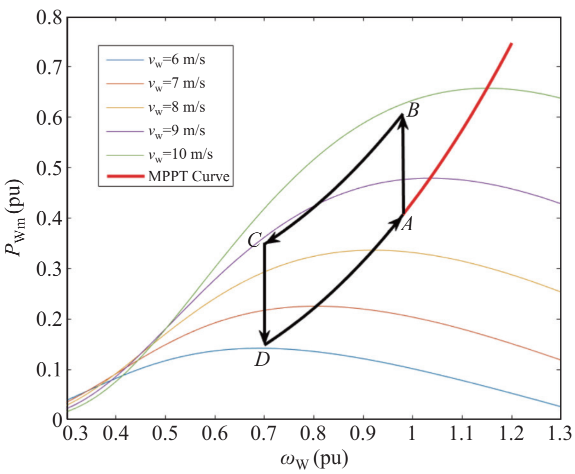

Fig. 2. Illustration of the entire process of participation of a wind turbine generator in power system frequency modulation when operating in MPPT mode.

The output of the auxiliary frequency control is:

$$\Delta P_{\text{We\_sig}} = -K_{\text{WD}}\Delta f - K_{\text{WI}}\frac{\mathrm{d}\Delta f}{\mathrm{d}t} \tag{1}$$

Adding the additional power $\Delta P_{\text{We\_sig}}$ to the reference power for MPPT control $P_{\text{We0\_sig}}$, we obtain the total power order $P_{\text{We\_sig}} = \Delta P_{\text{We\_sig}} + P_{\text{We0\_sig}}$.

We adopt MPPT control so that the power output is determined by the WTG rotor speed. Then, the reference power for MPPT control is a function of the rotor speed of the WTG.

$$P_{\text{We0\_sig}} = \mathrm{g}(\omega_{\mathrm{W}}) \tag{2}$$

The relationship between the power order $P_{\text{We\_sig}}$ and the actual power output P_{We} is modeled with a converter, and the equations are shown in appendix A.

The rotor motion equation of the WTG is:

$$T_{\text{JW}}\omega_{\mathrm{W}}\frac{\mathrm{d}\omega_{\mathrm{W}}}{\mathrm{d}t} = P_{\text{Wm}} - P_{\text{We}} \tag{3}$$

where T_{JW} is the WTG rotor inertia time constant.

Regardless of the adjustment of the pitch angle, assuming that the wind speed does not change during the period in which the WTG engages in the frequency regulation, the wind power captured by the wind turbine P_{Wm} is only related to the rotor speed of the WTG ω_{W} [22].

$$P_{\text{Wm}} = f(\omega_{\mathrm{W}}) \tag{4}$$

Detailed parameters are shown in appendix B.

III. Effect of Virtual Inertia Control on Max-ROCOF

The effect of WTG virtual inertia control on Max-ROCOF is studied in this section.

According to [23], the expression of the inertia response of SG is:

$$P_{\mathrm{e}}(t) \approx -\frac{P_{\mathrm{N}}T_{\mathrm{JS}}}{f_{\mathrm{N}}}\frac{\mathrm{d}f(t)}{\mathrm{d}t} \tag{5}$$

The inertia response of SG has no time delay. When a disturbance occurs and system frequency begins to drop, the kinetic energy stored in the rotor of SG will release immediately. Virtual inertia control is designed to simulate the inertia response of the SG.

However, the control link of the converter has a time delay. It can be approximated as a first-order inertial segment:

$$\Delta P_{\text{We}}(s) = \frac{1}{1+sT_{\text{inv}}}\Delta P_{\text{We\_sig}}(s) \tag{6}$$

A simulation to verify the rationality of the model approximation is conducted. In the detailed model, we change the WTG power reference P_{ref} with a step signal of magnitude 0.1, and the WTG output electric power is shown as Fig. 3. From Fig. 3 we know that using a first-order inertial segment as the simplified model of the converter is reasonable [24]. With the simplified model of the converter, the system model is also simplified, as shown in Fig. 4.

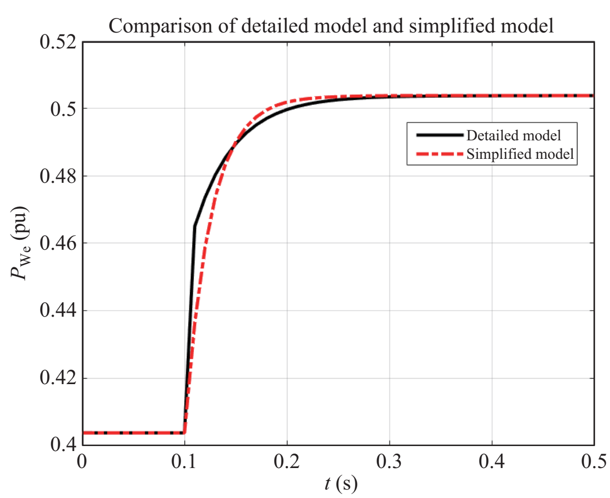

Fig. 3. WTG output electric power.

Based on the simplified analysis system in Fig. 4, the frequency response is subjected to a step power disturbance

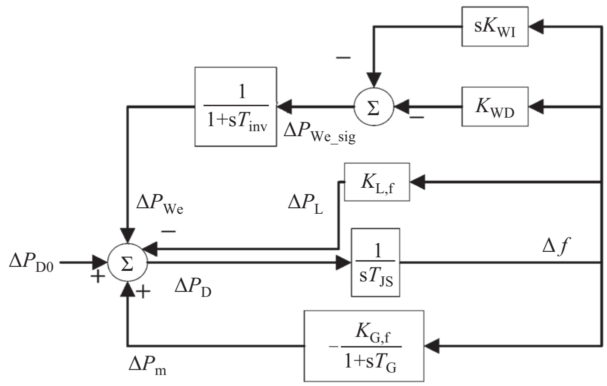

Fig. 4. Block diagram of simplified system.

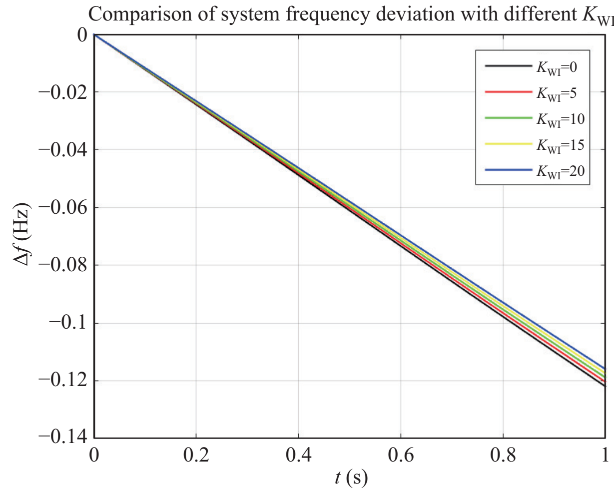

Fig. 5. Comparison of System Frequency Deviation with Different K_{WI}.

of magnitude ΔP_{D0} which is:

$$\Delta f(s)=\frac{\Delta P_{\mathrm{D0}}}{s}\cdot\frac{1}{K_{\mathrm{L,\,f}}+sT_{\mathrm{JS}}+\dfrac{K_{\mathrm{G,\,f}}}{1+sT_{\mathrm{G}}}+\dfrac{K_{\mathrm{WD}}+\mathrm{s}K_{\mathrm{WI}}}{1+sT_{\mathrm{inv}}}} \tag{7}$$

The Max-ROCOF occurs in the initial stage of the disturbance. Using the Laplace transform initial value theorem, we easily obtain:

$$\begin{aligned}\left.\frac{\mathrm{d}\Delta f(t)}{\mathrm{d}t}\right|_{t=0} &= \lim_{s\to\infty} s^2\cdot\Delta f(s)\\ &= \lim_{s\to\infty} s^2\cdot\frac{\Delta P_{\mathrm{D0}}}{s}\cdot\frac{1}{K_{\mathrm{L,\,f}}+sT_{\mathrm{JS}}+\dfrac{K_{\mathrm{G,\,f}}}{1+sT_{\mathrm{G}}}+\dfrac{K_{\mathrm{W1}}+\mathrm{s}K_{\mathrm{W2}}}{1+sT_{\mathrm{inv}}}}\\ &= \frac{\Delta P_{\mathrm{D0}}}{T_{\mathrm{JS}}}\end{aligned} \tag{8}$$

We can see that the Max-ROCOF (initial ROCOF) is hardly affected by the virtual inertia control of the WTG because of the first-order inertia link time delay. It is affected by the system's initial power disturbance ΔP_{D0} and the inertia time constant of the synchronous generator (SG) rotor T_{JS}.

This conclusion can be verified by simulation results with the detailed model. In the detailed model, the SG adopts the six-order model, and the WTG adopts the detailed converter model. The description of the six-order detailed model of the SG is shown in appendix C. We use a different K_{WI} for the simulation and calculate the Max-ROCOF, which is also the initial ROCOF.

From Fig. 5 and Table I, we know that with the increase of K_{WI}, Max-ROCOF remains unchanged.

TABLE I
MAX-ROCOF WITH DIFFERENT

K_{wI}	MAX-ROCOF
0	−0.1217
5	−0.1217
10	−0.1217
15	−0.1217
20	−0.1217

From the above analysis, we can conclude that virtual inertia control of the WTG has little effect on the Max-ROCOF.

IV. Optimization Study of WTG Auxiliary Frequency Control

Frequency deviation is an important index of the SFR. This section analyzes the role of virtual inertia control in reducing frequency deviation.

We start our study with the optimization of the auxiliary frequency control of the WTG with virtual inertia control and frequency droop control. The following is a detailed description of the optimization. The decision variables are K_{WI} and K_{WD} in (1). The objective function maximizes the frequency nadir after a step power disturbance. Equation (9) is equivalent to the optimizing frequency deviation.

$$\max_{K_{\mathrm{WI}},K_{\mathrm{WD}}}\left(\min_{t}\Delta f(t)\right) \tag{9}$$

The constraint is (10) according to the physical meaning of the frequency droop control and virtual inertia control.

$$K_{\mathrm{WD}}\geqslant 0, K_{\mathrm{WI}}\geqslant 0 \tag{10}$$

The frequency response in (9) is determined by the system in Fig. 1. Since it is a parameter optimization problem and no analytical expression of the objective function is available, we should use heuristic optimization algorithms to solve the problem. Thus, the particle swarm optimization algorithm is used to solve the problem. The optimal parameters and its comparison with other parameters are shown in Table II.

TABLE II
MAX-ROCOF WITH DIFFERENT

K_{WD}	K_{WI}	$\min\Delta f$
13.3	0	−0.9711 (optimal parameters)
13.3	5	−0.9841
13.3	10	−0.9972
0	0	−1.082 (no auxiliary frequency control)

Notice that the coefficient of virtual inertia control is zero, which means the virtual inertia control can be omitted.

The comparisons between the system responses with different coefficients are shown in Fig. 6. It can be seen that the SFR with an auxiliary controller with no virtual inertia control is the best result.

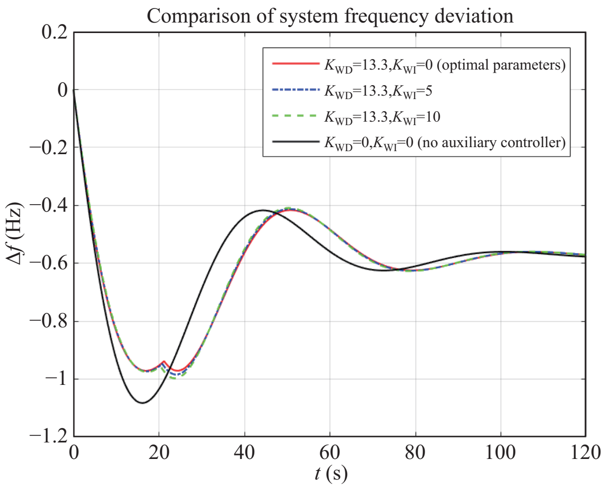

Fig. 6. The comparisons between SFRs with different parameters of controllers.

More cases are simulated to verify the conclusion. Case group 1 simulates disturbances of different magnitudes. Case group 2 and 3 simulate different proportions of the WTG. Case group 4 simulates different responding speeds of the PFC of the SG. Other parameters remain unchanged. The results are shown in Table III. In all cases in Table III, the optimal K_{WI} are all 0.

TABLE III
RESULTS OF OPTIMIZATION OF DROOP CONTROL AND VIRTUAL INERTIA CONTROL WITH DIFFERENT PARAMETERS

Case Group Number	Changed Parameter (s)	Optimization Results		$\min \Delta f$
		K_{WD}	K_{WI}	
1	$\Delta P_{\mathrm{D0}} = -1.12$	10.2	0	-1.3258
	$\Delta P_{\mathrm{D0}} = -0.98$	11.5	0	-1.1485
	$\Delta P_{\mathrm{D0}} = -0.70$	15.6	0	-0.7957
2	$T_{\mathrm{JS}} = 300$	13.2	0	-1.0104
	$T_{\mathrm{JS}} = 400$	13.3	0	-0.9319
	$T_{\mathrm{JS}} = 450$	13.4	0	-0.9012
3	$T_{\mathrm{JW}} = 15$	12.6	0	-0.9855
	$T_{\mathrm{JW}} = 20$	14.5	0	-0.9466
	$T_{\mathrm{JW}} = 25$	16.2	0	-0.9113
4	$T_{\mathrm{G}} = 10$	15.8	0	-0.8241
	$T_{\mathrm{G}} = 13$	14.2	0	-0.9154
	$T_{\mathrm{G}} = 18$	12.1	0	-1.0489

The following is an explanation of the above results. When the virtual inertia control is adopted, $\frac{\mathrm{d}\Delta f}{\mathrm{d}t}$ is relatively larger in the initial stage, and the control causes the WTG to quickly output more electric power. But the capability of the WTG to provide additional power is limited. If the capability of the WTG is released too quickly in the initial stage, the frequency deviation is suppressed and the PFC of the SG, which reacts to the frequency deviation, is restrained. When the capability of the WTG is exhausted, the action of the SG is not sufficient, which is detrimental to the frequency deviation. Therefore, virtual inertia control can be omitted for optimal frequency deviation.

V. FURTHER IMPROVEMENT OF FREQUENCY DROOP CONTROL

The importance of coordination between the WTG and SG is addressed in Section IV, which considered that the speed of releasing the frequency modulation energy of the WTG should assume an appropriate value. Section V now studies whether SFR will improve if the WTG releases frequency modulation energy at a slower speed and better coordinates with the SG.

To cause the WTG to release energy slower, a first-order inertial segment is added in the frequency droop control of the WTG, and the auxiliary frequency control assumes the following form:

$$\frac{\mathrm{d}\Delta P_{\mathrm{We\_sig}}}{\mathrm{d}t} = -\frac{1}{T_{\mathrm{WD}}}(\Delta P_{\mathrm{We\_sig}} + K_{\mathrm{WD}}\Delta f) \tag{11}$$

We call (11) the "frequency droop control with first-order inertial segment." T_{WD} is the time constant. Correspondingly, the block diagram of the auxiliary control of the WTG is modified as shown in Fig. 7.

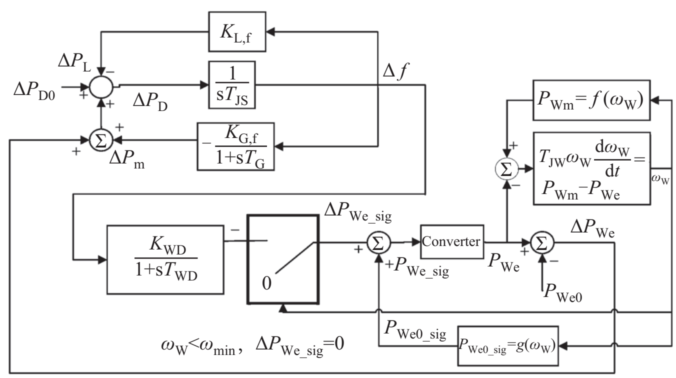

Fig. 7. Block diagram of droop control with time delay of the wind turbine generator.

Using $K_{\mathrm{WD}} = 13.3$ from Table II, we change the value of T_{WD} to obtain the relationship between $\min \Delta f$ and T_{WD} in Fig. 8. From Fig. 8, we can see that when $T_{\mathrm{WD}} = 1.3$, $\min \Delta f$ obtains its maximum value of -0.9675, which is larger than the value -0.9711 in Table II.

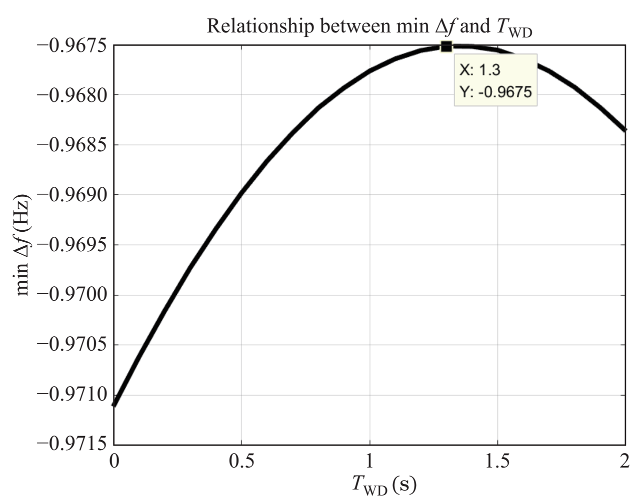

Fig. 8. Relationship between Δf and T_{WD}.

The comparisons between SFR with different K_{WD} and $T_{\mathrm{WD}}$are shown in Fig. 9. It can be seen from the optimal curve (red) that WTG releases energy for a longer period than the non-optimal curve (blue).

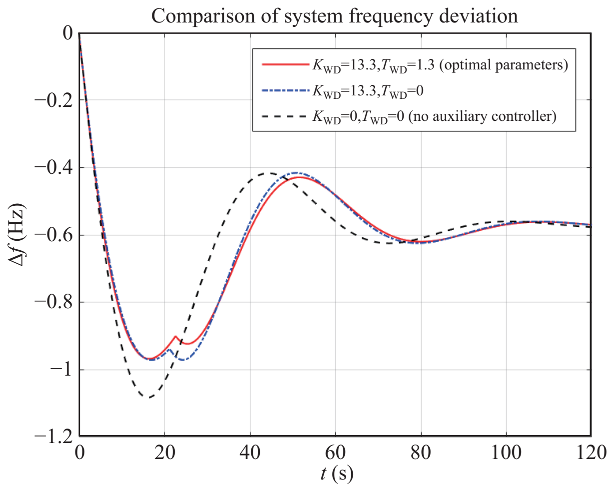

Fig. 9. The comparisons between SFRs with the auxiliary controller of optimal parameters and other parameters, and without controller.

For each of the optimal K_{WD} in Table III, the optimal T_{WD} is searched to further verify our assumption. The results are shown in Table IV. From Table IV we can see that droop control with the proper time delay is better than simple droop control. Therefore, the WTG does not need to release its limited frequency regulation capability too quickly. This finding further proves that coordination between the WTG and SG is important for better SFR.

TABLE IV
RESULTS OF OPTIMIZATION OF DROOP CONTROL WITH TIME DELAY USING DIFFERENT PARAMETERS

Case Group Number	Changed Parameter(s)	K_{WD}	T_{WD}	min Δf	min Δf in Table III
1	$\Delta P_{\mathrm{D0}}=-1.12$	10.2	1.2	−1.3225	−1.3258
	$\Delta P_{\mathrm{D0}}=-0.98$	11.5	1.3	−1.1451	−1.1485
	$\Delta P_{\mathrm{D0}}=-0.70$	15.6	1.4	−0.7919	−0.7957
2	$T_{\mathrm{JS}}=300$	13.2	1.1	−1.0074	−1.0104
	$T_{\mathrm{JS}}=400$	13.3	1.7	−0.9277	−0.9319
	$T_{\mathrm{JS}}=450$	13.4	2.1	−0.8963	−0.9012
3	$T_{\mathrm{JW}}=15$	12.6	1.5	−0.9811	−0.9855
	$T_{\mathrm{JW}}=20$	14.5	1.0	−0.9435	−0.9466
	$T_{\mathrm{JW}}=25$	16.2	0.7	−0.9101	−0.9113
4	$T_{\mathrm{G}}=10$	15.8	1.1	−0.8215	−0.8241
	$T_{\mathrm{G}}=13$	14.2	1.2	−0.9122	−0.9154
	$T_{\mathrm{G}}=18$	12.1	1.5	−1.0447	−1.0489

VI. CONCLUSIONS

A better design idea for an auxiliary frequency control scheme of a WTG is explored in this paper. The main contributions of this paper are as follows:

1) When the delay effect in the internal control of the WTG is considered and approximated as the first order inertial link, the virtual inertia control of the WTG has little effect on the Max-ROCOF.

2) If a WTG operates in a maximum power point tracking (MPPT) mode and uses the rotor deceleration for frequency modulation, its optimal auxiliary frequency control will contain only droop control. Furthermore, if a first-order inertial segment is added to the frequency droop control of the WTG, SFR can be even better.

3) Coordination between the WTG and SG is an important factor in designing the auxiliary frequency control of the WTG. Limited frequency modulation capability for the WTG is necessary for proper release.

Furthermore, as stated in [16], the SGs and power electronic interfaces (PEIs) have a completely different inherent frequency regulation mechanism. We should broaden our ideas to design a better auxiliary frequency control scheme for the WTG.

APPENDIX

A. Detailed Model of Converter

The relationship between the power order $P_{\mathrm{We\_sig}}$ and the actual power output P_{We} is modeled with a converter, and the equations are (A1)–(A24).

$$\frac{\mathrm{d}i_{\mathrm{x}}}{\mathrm{d}t}=\frac{\omega_0}{X_{\mathrm{f}}}\left(-R_{\mathrm{f}}i_{\mathrm{x}}+X_{\mathrm{f}}i_y+E_{\mathrm{x}}-u_{\mathrm{x}}\right) \tag{A1}$$

$$\frac{\mathrm{d}i_{\mathrm{y}}}{\mathrm{d}t}=\frac{\omega_0}{X_{\mathrm{f}}}\left(-R_{\mathrm{f}}i_{\mathrm{y}}-X_f i_{\mathrm{x}}+E_{\mathrm{y}}-u_y\right) \tag{A2}$$

$$\frac{\mathrm{d}x_{\mathrm{theta}}}{\mathrm{d}t}=u_{\mathrm{q}} \tag{A3}$$

$$\frac{\mathrm{d}\theta}{\mathrm{d}t}=k_{\mathrm{p_{pll}}}u_{\mathrm{q}}+k_{\mathrm{i_{pll}}}x_{\mathrm{theta}} \tag{A4}$$

$$\frac{\mathrm{d}x_{\mathrm{p}}}{\mathrm{d}t}=P_{\mathrm{ref}}-P_{\mathrm{We}} \tag{A5}$$

$$\frac{\mathrm{d}x_{\mathrm{q}}}{\mathrm{d}t}=-\left(Q_{\mathrm{ref}}-Q_{\mathrm{We}}\right) \tag{A6}$$

$$\frac{\mathrm{d}x_{\mathrm{id}}}{\mathrm{d}t}=i_{\mathrm{dref}}-i_{\mathrm{d}} \tag{A7}$$

$$\frac{\mathrm{d}x_{\mathrm{iq}}}{\mathrm{d}t}=i_{\mathrm{qref}}-i_{\mathrm{q}} \tag{A8}$$

$$\frac{\mathrm{d}\varphi}{\mathrm{d}t}=2\pi f_0\Delta f \tag{A9}$$

$$i_{\mathrm{dref}}=k_{\mathrm{p_p}}(P_{\mathrm{ref}}-P_{\mathrm{We}})+k_{\mathrm{i_p}}x_{\mathrm{p}} \tag{A10}$$

$$i_{\mathrm{qref}}=k_{\mathrm{p_q}}\left(-Q_{\mathrm{ref}}+Q_{\mathrm{We}}\right)+k_{\mathrm{i_q}}x_{\mathrm{q}} \tag{A11}$$

$$E_{\mathrm{d}}=k_{\mathrm{p_{id}}}\left(i_{\mathrm{dref}}-i_{\mathrm{d}}\right)+k_{\mathrm{i_{id}}}x_{\mathrm{id}}+u_{\mathrm{d}}-X_{\mathrm{f}}i_{\mathrm{q}} \tag{A12}$$

$$E_{\mathrm{q}}=k_{\mathrm{p_{iq}}}\left(i_{\mathrm{qref}}-i_{\mathrm{q}}\right)+k_{\mathrm{i_{iq}}}x_{\mathrm{iq}}+u_{\mathrm{q}}+X_{\mathrm{f}}i_{\mathrm{d}} \tag{A13}$$

$$u_{\mathrm{x}}=U_0\cos\varphi \tag{A14}$$

$$u_{\mathrm{y}}=U_0\sin\varphi \tag{A15}$$

$$P_{\mathrm{We}}=u_{\mathrm{x}}i_{\mathrm{x}}+u_{\mathrm{y}}i_{\mathrm{y}} \tag{A16}$$

$$Q_{\mathrm{We}}=u_{\mathrm{y}}i_{\mathrm{x}}-u_{\mathrm{x}}i_{\mathrm{y}} \tag{A17}$$

$$i_{\mathrm{d}}=i_{\mathrm{x}}\cos\theta+i_{\mathrm{y}}\sin\theta \tag{A18}$$

$$i_{\mathrm{q}}=-i_{\mathrm{x}}\sin\theta+i_{\mathrm{y}}\cos\theta \tag{A19}$$

$$u_{\mathrm{d}}=u_{\mathrm{x}}\cos\theta+u_{\mathrm{y}}\sin\theta \tag{A20}$$

$$u_{\mathrm{q}}=-u_{\mathrm{x}}\sin\theta+u_{\mathrm{y}}\cos\theta \tag{A21}$$

$$E_{\mathrm{x}}=E_{\mathrm{d}}\cos\theta-E_{\mathrm{q}}\sin\theta \tag{A22}$$

$$E_{\mathrm{y}}=E_{\mathrm{d}}\sin\theta+E_{\mathrm{q}}\cos\theta \tag{A23}$$

$$P_{\mathrm{ref}} = P_{\mathrm{We\_sig}} = P_{\mathrm{We0\_sig}} + \Delta P_{\mathrm{We\_sig}} \tag{A24}$$

B. Parameters of the Detailed Analysis Model

We assume that the wind speed is approximately unchanged when the WTG engages in the frequency regulation process, and the pitch angle adjustment is not activated. The blocks and parameters of Fig. 1 are described in detail in the following.

According to reference [25],

$$P_{\mathrm{Wm}} = f(\omega_{\mathrm{W}}) = \frac{1}{2}\pi\rho R^2 \nu_{\mathrm{W}}^3 C_{\mathrm{p}}(\lambda, \beta) \tag{B1}$$

where ρ is the air density, R is the rotor blade radius, ν_{W} is the wind speed, λ is the tip speed ratio, β is the pitch angle, and C_{p} is the power coefficient.

The tip speed ratio can be determined as follows.

$$\lambda = \frac{\omega_t R}{\nu_{\mathrm{W}}} = k_{\mathrm{G}} R \frac{\omega_{\mathrm{W}}}{\nu_{\mathrm{W}}} \tag{B2}$$

where $\mathrm{k_G}$ is the gear ratio of the gearbox. ω_t and ω_{W} are the wind turbine and WTG rotational speed, respectively.

The expression of C_{p} is as follows,

$$C_{\mathrm{p}} = 0.22\left(\frac{116}{\lambda_i} - 0.4\beta - 5\right)\mathrm{e}^{\frac{-12.5}{\lambda_i}} \tag{B3}$$

$$\lambda_i = \cfrac{1}{\cfrac{1}{(\lambda + 0.08\beta)} - \cfrac{0.035}{(\beta^3 + 1)}} \tag{B4}$$

The pitch angle is $\beta = 0$.

Using calculus, it can be easily obtained that C_{p} takes the maximum value $C_{\mathrm{p\,max}}$ when $\lambda = \lambda_{C_{\mathrm{p\,max}}}$. Substituting (B. 3) in (B. 1) yields:

$$P_{\mathrm{Wm\,max}} = \frac{1}{2}\pi\rho R^2 \left(\frac{\mathrm{k_G} R \omega_{\mathrm{W}}}{\lambda_{C_{\mathrm{p\,max}}}}\right)^3 C_{\mathrm{p\,max}} = K_{\mathrm{opt}} \omega_{\mathrm{W}}^3 \tag{B5}$$

According to the relevant data for wind turbines and wind farms, in our simulation, it can be approximated that $\frac{1}{2}\pi\rho R^2 = 0.0015$ and $\mathrm{k_G} R = 55$. The wind speed is set as $\nu_{\mathrm{W}} = 8.5$ m/s.

Therefore, in Fig. 1,

$$f(\omega_{\mathrm{W}}) = 0.314\left(\frac{17.93}{\omega_{\mathrm{W}}} - 9.06\right)\mathrm{e}^{\frac{-1.932}{\omega_{\mathrm{W}}}} \tag{B6}$$

$$\mathrm{g}(\omega_{\mathrm{W}}) = 0.4322\omega_{\mathrm{W}}^3 \tag{B7}$$

The other parameters of the system are shown in the following.

$$\begin{aligned} &T_{\mathrm{JS}} = 345.15, T_{\mathrm{JW}} = 16.72, K_{\mathrm{L,\,f}} = 5.468, K_{\mathrm{G,\,f}} = 67.5,\\ &T_{\mathrm{G}} = 15, \omega_{\min} = 0.7, \Delta P_{\mathrm{D0}} = -0.84, \omega_0 = 100\pi,\\ &R_{\mathrm{f}} = 0.01, X_{\mathrm{f}} = 0.1, Q_{\mathrm{ref}} = 0, k_{\mathrm{p_{pll}}} = 50, k_{\mathrm{i_{pll}}} = 1000,\\ &k_{\mathrm{p_p}} = 1, k_{\mathrm{i_p}} = 50, k_{\mathrm{p_q}} = 1, k_{\mathrm{i_q}} = 50, k_{\mathrm{p_{id}}} = 1, k_{\mathrm{i_{id}}} = 100,\\ &k_{\mathrm{p_{iq}}} = 1, k_{\mathrm{i_{iq}}} = 100 \end{aligned} \tag{B8}$$

C. Six-Order Detailed Model of Synchronous Generator

The six-order detailed model of a SG is (C1)–(C24)

$$\frac{\mathrm{d}\delta}{\mathrm{d}t} = 2\pi f_0 \Delta f \tag{C1}$$

$$\frac{\mathrm{d}\Delta f}{\mathrm{d}t} = \frac{1}{T_{\mathrm{JS}}}\left(\Delta P_{\mathrm{D0}} + \Delta P_{\mathrm{m}} - \Delta P_{\mathrm{e}} - \Delta P_{\mathrm{L}} + \Delta P_{\mathrm{We}}\right) \tag{C2}$$

$$\frac{\mathrm{d}\varphi_{\mathrm{fd}}}{\mathrm{d}t} = \frac{R_{\mathrm{fd}}}{X_{\mathrm{ad}}} E_{\mathrm{fd}} - R_{\mathrm{fd}} i_{\mathrm{fd}} \tag{C3}$$

$$\frac{\mathrm{d}\varphi_{\mathrm{d'}}}{\mathrm{d}t} = -R_{\mathrm{d'}} i_{\mathrm{d'}} \tag{C4}$$

$$\frac{\mathrm{d}\varphi_{\mathrm{d'}}}{\mathrm{d}t} = -R_{\mathrm{d'}} i_{\mathrm{d'}} \tag{C5}$$

$$\frac{\mathrm{d}\varphi_{\mathrm{q''}}}{\mathrm{d}t} = -R_{\mathrm{q''}} i_{\mathrm{q''}} \tag{C6}$$

$$\frac{\mathrm{d}E_{\mathrm{fd}}}{\mathrm{d}t} = \frac{1}{T_{\mathrm{A}}}\left[-E_{\mathrm{fd}} + K_{\mathrm{A}}(U_{\mathrm{ref}} - U_{\mathrm{t}} + p_2)\right] \tag{C7}$$

$$\frac{\mathrm{d}p_1}{\mathrm{d}t} = \frac{1}{T_{\mathrm{W}}}\left(-p_1 + K_{\mathrm{STAB}} T_{\mathrm{W}} \frac{\mathrm{d}\Delta f}{\mathrm{d}t}\right) \tag{C8}$$

$$\frac{\mathrm{d}p_2}{\mathrm{d}t} = \frac{1}{T_2}\left(-p_2 + p_1 + T_1 \frac{dp_1}{\mathrm{d}t}\right) \tag{C9}$$

$$u_{\mathrm{d}} = X_{\mathrm{q}} i_{\mathrm{q}} - X_{\mathrm{aq}} i_{\mathrm{d'}} - X_{\mathrm{aq}} i_{\mathrm{q''}} \tag{C10}$$

$$u_{\mathrm{q}} = -X_{\mathrm{d}} i_{\mathrm{d}} + X_{\mathrm{ad}} i_{\mathrm{fd}} + X_{\mathrm{ad}} i_{\mathrm{d'}} \tag{C11}$$

$$\varphi_{\mathrm{fd}} = -X_{\mathrm{ad}} i_{\mathrm{d}} + X_{\mathrm{ffd}} i_{\mathrm{fd}} + X_{\mathrm{ad}} i_{\mathrm{d'}} \tag{C12}$$

$$\varphi_{\mathrm{d'}} = -X_{\mathrm{ad}} i_{\mathrm{d}} + X_{\mathrm{ad}} i_{\mathrm{fd}} + X_{\mathrm{d''}} i_{\mathrm{d'}} \tag{C13}$$

$$\varphi_{\mathrm{d'}} = -X_{\mathrm{aq}} i_{\mathrm{q}} + X_{\mathrm{q''}} i_{\mathrm{d'}} + X_{\mathrm{aq}} i_{\mathrm{q''}} \tag{C14}$$

$$\varphi_{\mathrm{q''}} = -X_{\mathrm{aq}} i_{\mathrm{q}} + X_{\mathrm{aq}} i_{\mathrm{d'}} + X_{\mathrm{q''}} i_{\mathrm{q''}} \tag{C15}$$

$$i_{\mathrm{x}} = i_{\mathrm{d}} \sin\delta + i_{\mathrm{q}} \cos\delta \tag{C16}$$

$$i_{\mathrm{y}} = -i_{\mathrm{d}} \cos\delta + i_{\mathrm{q}} \sin\delta \tag{C17}$$

$$U_{\mathrm{tc}} = V_{\mathrm{s}} + \mathrm{j} X_{\mathrm{L}}(i_{\mathrm{x}} + \mathrm{j} i_{\mathrm{y}}) \tag{C18}$$

$$U_{\mathrm{t}} = |U_{\mathrm{tc}}| \tag{C19}$$

$$u_{\mathrm{x}} = Re(U_{\mathrm{tc}}) \tag{C20}$$

$$u_{\mathrm{y}} = Im(U_{\mathrm{tc}}) \tag{C21}$$

$$u_{\mathrm{d}} = u_{\mathrm{x}} \sin\delta - u_{\mathrm{y}} \cos\delta \tag{C22}$$

$$u_{\mathrm{q}} = u_{\mathrm{x}} \cos\delta + u_{\mathrm{y}} \sin\delta \tag{C23}$$

$$P_{\mathrm{e}} = u_{\mathrm{d}} i_{\mathrm{d}} + u_{\mathrm{q}} i_{\mathrm{q}} \tag{C24}$$

REFERENCES

[1] G. P. Chen, M. J. Li, T. Xu, and M. S. Liu, “Study on technical bottleneck of new energy development,” *Proceedings of the CSEE*, vol. 37, no. 1, pp. 20–26, Jan. 2017.

[2] J. Ekanayake and N. Jenkins, “Comparison of the response of doubly fed and fixed-speed induction generator wind turbines to changes in network frequency,” *IEEE Transactions on Energy Conversion*, vol. 19, no. 4, pp. 800–802, Dec. 2004.

[3] A. Zertek, G. Verbic, and M. Pantos, “A novel strategy for variable-speed wind turbines’ participation in primary frequency control,” *IEEE Transactions on Sustainable Energy*, vol. 3, no. 4, pp. 791–799, Oct. 2012.

[4] K. V. Vidyanandan and N. Senroy, “Primary frequency regulation by deloaded wind turbines using variable droop,” *IEEE Transactions on Power Systems*, vol. 28, no. 2, pp. 837–846, May 2013.

[5] A. B. T. Attya and T. Hartkopf, “Control and quantification of kinetic energy released by wind farms during power system frequency drops,” *IET Renewable Power Generation*, vol. 7, no. 3, pp. 210–224, May 2013.

[6] G. Ramtharan, J. B. Ekanayake, and N. Jenkins, “Frequency support from doubly fed induction generator wind turbines,” *IET Renewable Power Generation*, vol. 1, no. 1, pp. 3–9, Mar. 2007.

[7] J. F. Conroy and R. Watson, “Frequency response capability of full converter wind turbine generators in comparison to conventional generation,” *IEEE Transactions on Power Systems*, vol. 23, no. 2, pp. 649–656, May 2008.

[8] D. Gautam, L. Goel, R. Ayyanar, V. Vittal, and T. Harbour, “Control strategy to mitigate the impact of reduced inertia due to doubly fed induction generators on large power systems,” *IEEE Transactions on Power Systems*, vol. 26, no. 1, pp. 214–224, Feb. 2011.

[9] S. Ghosh, S. Kamalasadan, N. Senroy, and J. Enslin, "Doubly fed induction generator (DFIG)-based wind farm control framework for primary frequency and inertial response application," *IEEE Transactions on Power Systems*, vol. 31, no. 3, pp. 1861–1871, May 2016.

[10] R. You, J. Y. Chai, X. D. Sun, and Y. L. Lin, "Variable speed wind turbine based on electromagnetic coupler and its experimental measurement, " in *2014 IEEE PES General Meeting | Conference & Exposition*, National Harbor, MD, 2014, pp. 1–5.

[11] J. Morren, S. W. H. de Haan, W. L. Kling, and J. A. Ferreira, "Wind turbines emulating inertia and supporting primary frequency control, " *IEEE Transactions on Power Systems*, vol. 21, no. 1, pp. 433–434, Feb. 2006.

[12] G. C. Tarnowski, P. C. Kjar, P. E. Sorensen, and J. Ostergaard, "Variable speed wind turbines capability for temporary over-production," in *2009 IEEE Power & Energy Society General Meeting*, Calgary, AB, 2009, pp. 1–7.

[13] M. Kayikci and J. V. Milanovic, "Dynamic contribution of DFIG-based wind plants to system frequency disturbances," *IEEE Transactions on Power Systems*, vol. 24, no. 2, pp. 859–867, May 2009.

[14] I. D. Margaris, S. A. Papathanassiou, N. D. Hatziargyriou, A. D. Hansen, and P. Sorensen, "Frequency control in autonomous power systems with high wind power penetration," *IEEE Transactions on Sustainable Energy*, vol. 3, no. 2, pp. 189–199, Apr. 2012.

[15] J. Lee, E. Muljadi, P. Srensen, and Y. C. Kang, "Releasable kinetic energy-based inertial control of a DFIG wind power plant," *IEEE Transactions on Sustainable Energy*, vol. 7, no. 1, pp. 279–288, Jan. 2016.

[16] Y. D. Ye, Y. Qiao, and Z. X. Lu, "Revolution of frequency regulation in the converter-dominated power system," *Renewable and Sustainable Energy Reviews*, vol. 111, pp. 145–156, Sep. 2019.

[17] G. Y. Xu, F. L. Liu, J. X. Hu, and T. S. Bi, "Coordination of wind turbines and synchronous generators for system frequency control," *Renewable Energy*, vol. 129, pp. 225–236, Dec. 2018.

[18] Y. Min, L. Chen, and Q. Jiang, *Power System Stability Analysis*, Beijing, China: Tsinghua University Press, 2016.

[19] L. Sun, Y. H. Hou, C. Y. Peng, and J. B. Hu, "Comparative studies on frequency responses of type 3 wind turbines and synchronous generators," in *2017 IEEE Power & Energy Society General Meeting*, Chicago, IL, USA, 2017, pp. 1–5.

[20] Y. J. Li, Z. Xu, and K. P. Wong, "Advanced control strategies of PMSG-based wind turbines for system inertia support," *IEEE Transactions on Power Systems*, vol. 32, no. 4, pp. 3027–3037, Jul. 2017.

[21] J. B. Hu, L. Sun, X. M. Yuan, S. Wang, and Y. N. Chi, "Modeling of type 3 wind turbines with df/dt inertia control for system frequency response study," *IEEE Transactions on Power Systems*, vol. 32, no. 4, pp. 2799–2809, Jul. 2017.

[22] S. Zhou and Z. Lu, *Wind Power and Power System*, Beijing, China: China Electric Power Press, 2011.

[23] X. H. Qin, L. N. Su, Y. N. Chi, Q. Guo, and X. W. Xu, "Functional orientation discrimination of inertia support and primary frequency regulation of virtual synchronous generator in large power grid, " *Automation of Electric Power Systems*, vol. 42, no. 9, pp. 36–43, May 2018.

[24] X. Guo, "Research on the auxiliary frequency regulation of VSC-HVDC systems with wind power integration," M. S. thesis, Department of Electrical Engineering, Tsinghua University, Beijing, China, 2018.

[25] Y. Li, "Advanced control strategies for renewable energy integration for system support," Ph. D. dissertation, Department of Electrical Engineering, The Hong Kong Polytechnic University, Hong Kong, China, 2017.

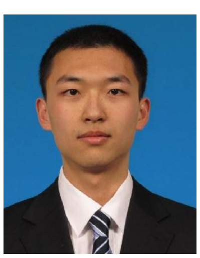

Ming Sun (S'16) received the B.S. degree in Electrical Engineering from the Department of Electrical Engineering at Tsinghua University, Beijing, China, in 2016 where he is currently pursuing the Ph.D. degree in Electrical Engineering. His research interests include power system frequency security and auxiliary frequency control of renewable energy.

Yong Min (S'84–M'90) received the B.S. and Ph.D. degrees in Electrical Engineering in the Department of Electrical Engineering from Tsinghua University, Beijing, China, in 1984 and 1990, respectively. He is currently a Professor in the Department of Electrical Engineering at Tsinghua University, Beijing, China. His research interests include power system dynamic analysis and smart grid technology. Prof. Min is a Fellow of the Institution of Engineering and Technology.

Lei Chen (S'03–M'08) received the B.Sc. and Ph.D. degrees in Electrical Engineering from Tsinghua University, Beijing, China, in 2003 and 2008, respectively. Since 2008, he has been with the Department of Electrical Engineering, Tsinghua University, where he is currently an Associate Professor. His research interests include dynamic analysis and control of power systems. He was a recipient of the Excellent Young Scientists Fund of the National Natural Science Foundation of China in 2019.

Kaiyuan Hou (S'96–M'01–M'05) received the B.Sc., M.S., and Ph.D. degrees in Electrical Engineering from Central China University of Science and Engineering, Northeast Electric Power University, and Tsinghua University, Beijing, China, in 1996, 2001, and 2005, respectively. His research interests include power grid dispatching operation, power grid security management, stability analysis and control.

Deming Xia (S'02–M'07) received the B.Sc. and Ph.D. degrees in Electrical Engineering from Tsinghua University, Beijing, China, in 2003 and 2008, respectively. His research interests include power system analysis and control, power grid dispatching technology, and new energy consumption.

Hangyin Mao received the M.Sc. degree in Electrical Engineering from Zhejiang University, Hangzhou, China, in 2010. His research interests include power systems and automation.